ISBN: 978-3-95450-227-1 ISSN: 2673-5490 doi:10.18429/JACoW-IPAC2022-WEPOPT035

OPTICS FOR STRONG HADRON COOLING IN EIC HSR-IR2

S. Peggs*, D. Xu, W.F. Bergan, D. Bruno, Y. Gao, D. Holmes, R. Lambiase, C. Liu, H. Lovelace III, G. Mahler, F. Micolon, V. Ptitsyn, G. Robert-Demolaize, Y. Than, J. Tuozzolo, E. Wang, D. Weiss, BNL, Upton, USA
S. Benson, T. Michalski, TJNAF, Newport News, USA

LAYOUT GEOMETRY

Strong Hadron Cooling (SHC) in the Hadron Storage Ring (HSR) [1] of the Electron-Ion Collider (EIC) uses microbunched electron cooling [2–9] to enable the highest luminosities. Figure 1 sketches the facility to be built in Insertion Region 2 (IR2) when the Relativistic Heavy Ion Collider (RHIC) is upgraded to become HSR. Electrons from an Energy Recovery Linac (ERL) co-move with hadrons as they pass through the Modulator straight (M). The imprint left by the hadrons on the electrons is amplified and then fed back to cool the hadrons as they co-move through the Kicker straight (K).

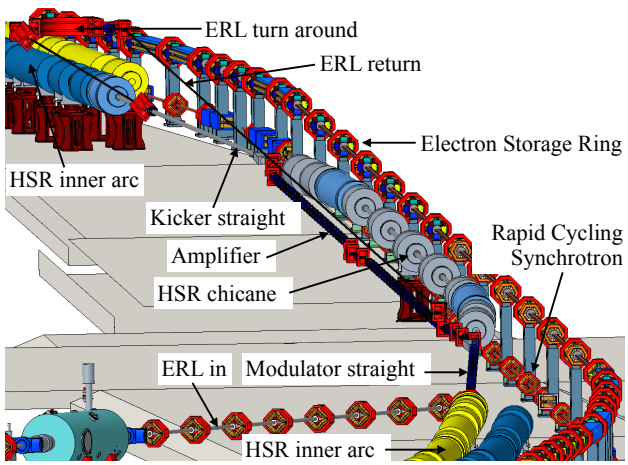

Figure 1: Hadrons and electrons co-move from bottom-right to top-left through the modulator and kicker straights. Electrons turn around and return to the ERL. IR2 is shared by two additional EIC accelerators – the Electron Storage Ring and the Rapid Cycling Synchrotron electron injector [10] – that do not participate in the cooling.

The "inner-arc-to-inner-arc" sequence shown in Fig. 2 is left-right symmetric in geometry and in optics [1]. RHIC magnets outside the IR-arc boundaries at quadrupoles Q10 (left and right) are unmoved, although they will be refurbished when RHIC becomes HSR.

COOLING RATES

Table 1 lists the primary optical parameters required and achieved in lattice HSR-220512a at two principal proton beam energies, 100 GeV and 275 GeV. Some intuition for their roles is gained by assuming that $\alpha_{x_0} = \alpha_{y_0} = D'_{x0} = D'_{y0} = 0$ at the K and M centers, and defining 3 cooling

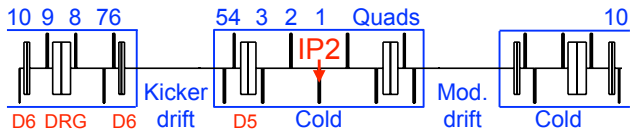

Figure 2: Left-right symmetric IR2 layout (to scale), with an isolated central cryostat and 4 warm-to-cold transitions. All quadrupoles are recycled from RHIC arcs with the same FODO cell spacing, except for doublets Q7-Q6 and Q5-Q4.

Table 1: Primary IR2 and ERL parameters. Subscript 0 and superscript star refer to the M and K straight centers and to the symmetry point IP2, respectively. Co-ordinate s advances from left to right.

Parameter	Unit	Proton energy [GeV]	
		100	275
Insertion Region 2			
Modulator/kicker length	m	39	39
Optics solution branch		JJ	DD
β_{x0}	m	40	40
α_{x0}		0	0
β_{y0}	m	~ 44	~ 60
α_{y0}		0	0
β^*_x	m	50	50
β^*_y	m	50	50
D_{x0} K & M	m	1.108	1.360
D'_{x0} slope at K		-0.0177	-0.0146
$\Delta\mu_x$ M-to-K phase adv.	rad	5.055	5.446
Chicane strength, $R_{56,h}$	mm	-6.35	-2.26
Energy Recovery Linac			
Electron energy	MeV	54.5	150
Charge	nC	1	1
Bunch length	mm	14	7
Peak Current	A	8.5	17
Average current	mA	100	100
Normalized emittance	μm	3	3
Slice rms $\Delta p/p$		$<1\times10^{-4}$	$<1\times10^{-4}$

coefficients [5, 11]

$$\begin{aligned} S_x &= (D_{x0}^2/\beta_{x0})\,\sin(\Delta\mu_x) \\ S_y &= (D_{y0}^2/\beta_{y0})\,\sin(\Delta\mu_y) \\ S_z &= R_{56}^h - S_x - S_y \end{aligned} \tag{1}$$

where the hadron chicane strength R_{56}^h follows the MADX sign convention. For *small* values of S the horizontal, vertical and longitudinal cooling rates are approximately

$$(\tau_x^{-1}, \tau_y^{-1}, \tau_z^{-1}) \approx C_\tau \cdot (S_x, S_y, S_z) \tag{2}$$

* peggs@bnl.gov

ISBN: 978-3-95450-227-1 ISSN: 2673-5490 doi:10.18429/JACoW-IPAC2022-WEPOPT035

where C_τ is a constant. When this approximation is valid *in the weak limit* the cooling rate sum is constant at

$$\tau_{sum}^{-1} \;=\; \tau_x^{-1} + \tau_y^{-1} + \tau_z^{-1} \;\approx\; C_\tau\, R_{56}^h \qquad (3)$$

Figure 3 (top) tests the prediction that the cooling rate sum is proportional to $-R_{56}^h$. Linearity holds true for $R_{56}^h > -3$ mm, but τ_{sum}^{-1} saturates at about 1 h^{-1} when $R_{56}^h \approx -4.5$ mm.

Vertical cooling requires significant vertical dispersion D_{y0} (see Eq. 1). Figure 3 (bottom) explores this in the 2D parameter plane (D_{y0}, R_{56}^h). A relatively broad saturation plateau is found at around $(D_{y0}, R_{56}^h) \approx (0.2\,[\mathrm{m}], -7\,[\mathrm{mm}])$. Preliminary studies show that such vertical dispersions can be generated by using RHIC-strength vertical closed orbit correctors in the two arcs on each side of IR2 to build up and damp down a local dispersion wave [12].

OPTICAL MATCHING

The geometric strengths k of quadrupoles Q1 through Q9 are varied to match the 9 SHC control parameters. Four strengths ($k9$ to $k6$) match the Q10 boundary conditions to the requisite $\beta_{x0}, \alpha_{x0}, \beta_{y0}, \alpha_{y0}$ values. Five strengths take care of β_x^*, β_y^* values at IP2, and ensure the symmetry conditions $\alpha_x^* = \alpha_y^* = D'^* = 0$. Thus IR2 optics are parameterized by a 6D optical vector $(\beta_{x0}, \alpha_{x0}, \beta_{y0}, \alpha_{y0}, \beta_x^*, \beta_y^*)$ that corresponds by a nonlinear transformation to a 6D SHC control space vector $(\beta_{x0}, \beta_{y0}, D_0, D_0', R_{56}^h, \Delta\mu)$.

All quads Q1 through Q9 are 1.11 m long arc quads, taken from the many that are available from the second RHIC ring, with a strength limit

$$|k| \;\lesssim\; 0.1\;\; [\mathrm{m}^{-2}] \qquad (4)$$

at the highest HSR energies. A global search with initial conditions all over a k-space hypercube of that size converges on 16 solution branches, all corresponding to a single point in SHC control space. These branches are evaluated with regard to 1) the hypervolume of SHC control space in which that branch converges, 2) the maximum β_x and β_y values, and 3) peak absolute and root mean square quadrupole strength values. This evaluation quickly reduces the set of practical branches to 4, labeled BB, DD, JJ and LL.

Figure 4 shows that branches DD and JJ cover a broad range of useful R_{56}^h values at 275 GeV, and an adequate range at 100 GeV. Strong Hadron Cooling at 41 GeV is no longer foreseen, because no solution branch works and because the corresponding ERL parameters are difficult to achieve. A 24 GeV PreCooler that is under consideration for inclusion in IR2 might also be able to cool 41 GeV protons [13].

Figure 5 records the Twiss function performance of the DD and JJ optics when $(\beta_{x0}, \alpha_{x0}, \beta_{y0}, \alpha_{y0}, \beta_x^*, \beta_y^*) = (40, 0, 60, 0, 50, 50)$ [lengths in meters]. Injection optics that reduce β_{max} to 163 m or less are available.

Longer kicker and modulator straights are preferable, since

$$\tau_{sum}^{-1} \;\propto\; L_{\mathrm{M}} L_{\mathrm{K}} \qquad (5)$$

However, longer drifts are harder to fit in the tunnel. The layout with 64 m straights shown in Fig. 6 (bottom) continues

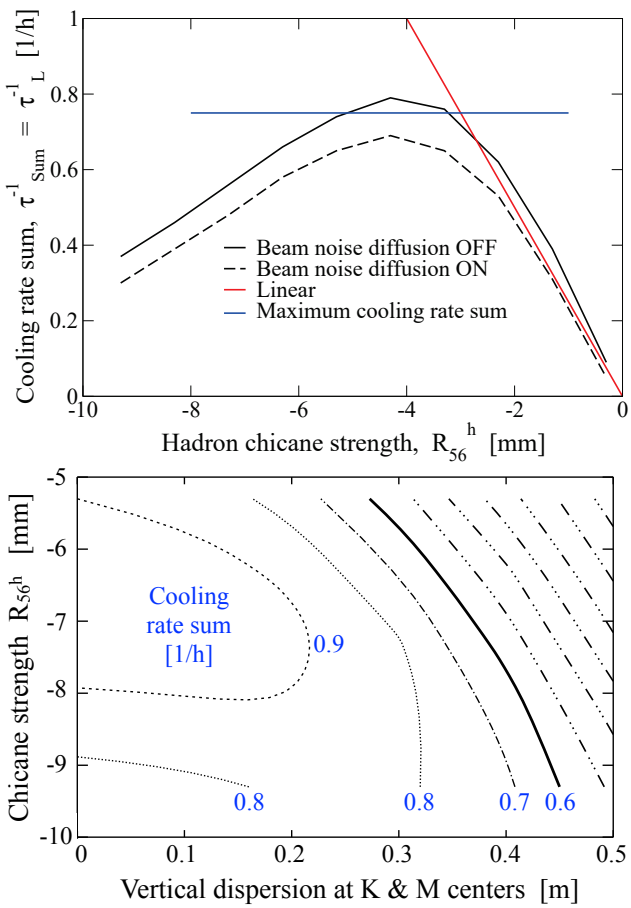

Figure 3: Top: Cooling rate sum vs R_{56}^h, with linearity for $R_{56}^h > -3$ mm and saturation at a sum rate approaching 1 h^{-1}. Horizontal and vertical dispersions are set to zero. Bottom: The rate sum in (D_{y0}, R_{56}^h) space reaches a maximum of almost 1 h^{-1} with a vertical dispersion of less than 0.2 m. See Table 1 for other parameters.

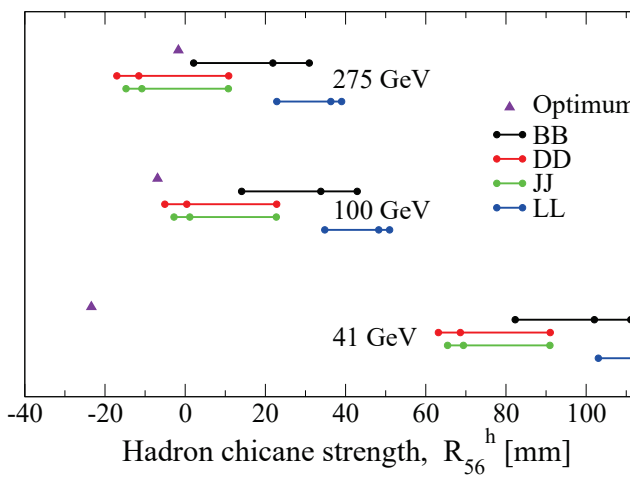

Figure 4: Chicane strength ranges available in the 4 most promising solution branches. No branch works at 41 GeV. The vertical axis merely separates the 3 energy datasets.

ISBN: 978-3-95450-227-1 ISSN: 2673-5490 doi:10.18429/JACoW-IPAC2022-WEPOPT035

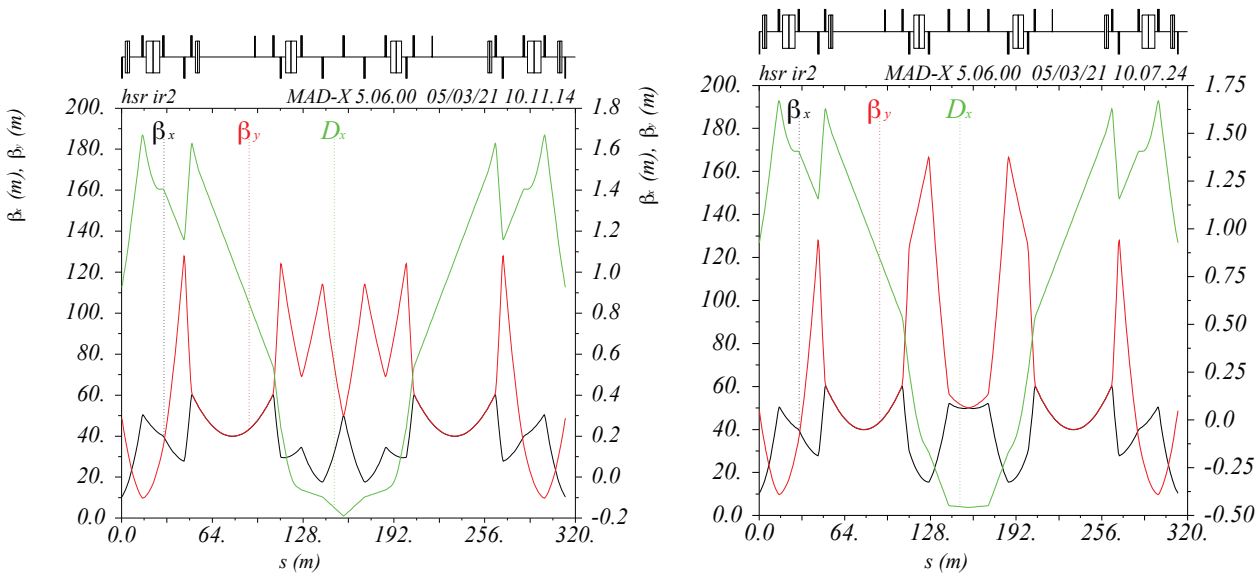

Figure 5: Typical cooling optics. Left: JJ(40,0,60,0,50,50) at 100 GeV. Right: DD(40,0,60,0,50,50) at 275 GeV.

to be evaluated, especially with respect to optical matching at 100 GeV. That layout bends earlier, but does not move IP2. A later more realistic lattice will include a Siberian snake, dipole correctors for large radial shifts, and various single and multi-layer correctors.

ENERGY RECOVERY LINAC

Electron micropulses in the ERL must be as long as feasible to overlap as much of the hadron bunches as possible. Optimal ERL parameters are summarized in Table 1, with more details in [7]. A bunch charge of 1 nC provides the required emittance and energy spread, but pushes the average current as far as realistically possible, to 100 mA. These parameters present multiple challenges.

A 400 kV high voltage DC gun with a multi-alkali photocathode is the only realistic option to produce such a large average current. The 5.6 MeV injector also includes a 197 MHz bunching section, a 591 MHz 1.8 cell SRF booster and a 1773 MHz linearizer cavity. The fundamental power couplers deliver as much as 600 kW, while the third harmonic cavity couples 60 kW from the beam to a load.

The accelerating and decelerating electron beams merge at the entrance to the LINAC. Simulations show that an accelerating emittance of 3 μm is maintained up to the first LINAC cavity with a merger dogleg made from two dipoles and two solenoids. Eight 5-cell 591 MHz SRF cavities, in separate cryomodules, each have an accelerating gap voltage of 20 MV. Three 1773 MHz SRF third harmonic cavities with a 10 MV gap voltage provide a very small rms energy spread with a very long bunch.

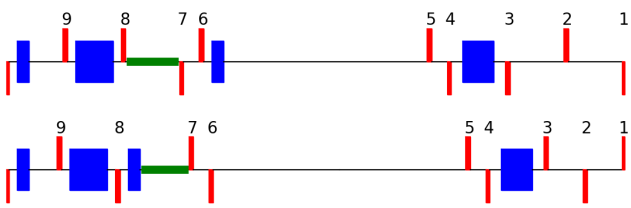

Figure 6: Lengthening the straights. Top: Current layout with 39 m straights. Bottom: an improved layout with 64 m straights. The green block is reserved for a Siberian snake.

The microbunching gain up to the cooler is nearly unity, maintaining the beam quality and keeping the electron beam noise near the level of shot noise. Isochronous and achromatic Bates bends [8] turn the beam through 180 degrees at the ERL ends, with a transverse size of less than 2.5 meters. Studies of halo and ion trapping effects continue for an ERL with an average current that is far higher than the current state-of-the-art.

CONCLUSIONS

A proof-of-principle layout and optics has been integrated into the lattice HSR-220512a, delivering good SHC control parameter ranges at 100 GeV and 275 GeV. Peak magnet strengths are consistent with re-purposed RHIC arc quadrupoles and RHIC insertion region dipoles. Twiss values are reasonable, and acceptable injection optics are available. The vertical dispersion values that are necessary for vertical cooling are reasonable, although their implementation needs further study. Engineering requirements and solutions continue to be evaluated in support of a 2022 cost and schedule estimate, re-using RHIC infrastructure (cryogenic, vacuum, magnets, et cetera) as much as possible. The potential use of a Ring Cooler alternative to Strong Hadron Cooling is also under study.

ACKNOWLEDGMENTS

Many thanks to our colleagues J.S. Berg, C. Cullen, A. Drees, A. Fedotov, B. Gamage, D. Kayran, and M. Valette.

ISBN: 978-3-95450-227-1 ISSN: 2673-5490 doi:10.18429/JACoW-IPAC2022-WEPOPT035

REFERENCES

[1] C. Liu *et al.*, "Reconfiguration of RHIC Straight Sections for the EIC", presented at the IPAC'22, Bangkok, Thailand, Jun. 2022, paper WEPOPT034, this conference.

[2] D. Ratner, "Microbunched electron cooling for high-energy hadron beams", *Phys. Rev. Lett.*, vol. 111, p. 084802, Aug. 2013. doi:10.1103/PhysRevLett.111.084802

[3] G. Stupakov, "Cooling rate for microbunched electron cooling without amplification", *Phys. Rev. Accel. Beams*, vol. 21, p. 114402, Nov. 2018. doi:10.1103/PhysRevAccelBeams.21.114402

[4] G. Stupakov and P. Baxevanis, "Microbunched electron cooling with amplification cascades", *Phys. Rev. Accel. Beams*, vol. 22, p. 034401, Mar. 2019. doi:10.1103/PhysRevAccelBeams.22.034401

[5] P. Baxevanis and G. Stupakov, "Transverse dynamics considerations for microbunched electron cooling", *Phys. Rev. Accel. Beams*, vol. 22, p. 081003, Aug. 2019. doi:10.1103/PhysRevAccelBeams.22.081003

[6] P. Baxevanis and G. Stupakov, "Hadron beam evolution in microbunched electron cooling", *Phys. Rev. Accel. Beams*, vol. 23, p. 111001, Nov. 2020. doi:10.1103/PhysRevAccelBeams.23.111001

[7] E. Wang *et al.*, "The Accelerator Design Progress for EIC Strong Hadron Cooling", in *Proc. IPAC'21*, Campinas, Brazil, May 2021, pp. 1424–1427. doi:10.18429/JACoW-IPAC2021-TUPAB036

[8] W.F. Bergan, "Improvements to Simulations of Microbunched Electron Cooling for the EIC", in *Proc. COOL'21*, Novosibirsk, Russia, Nov. 2021, pp. 103–106. doi:10.18429/JACoW-COOL2021-P2008

[9] W. F. Bergan, P. Baxevanis, M. Blaskiewicz, G. Stupakov, and E. Wang, "Design of an MBEC Cooler for the EIC", in *Proc. IPAC'21*, Campinas, Brazil, May 2021, pp. 1819–1822. doi:10.18429/JACoW-IPAC2021-TUPAB179

[10] H. Lovelace III, C. Montag, V. H. Ranjbar, and F. Lin, "The EIC Rapid Cycling Synchrotron Dynamic Aperture Optimization", presented at the IPAC'22, Bangkok, Thailand, Jun. 2022, paper MOPOST055, this conference.

[11] V. Lebedev, "Optical stochastic cooling", *ICFA Beam Dyn. Newslett.*, vol. 65, p. 100, 2014.

[12] S. Peggs, unpublished, 2022.

[13] S. Benson *et al.*, "Low Energy Cooling for the Electron Ion Collider", EIC-HDR-TN-012, 2020. doi:10.2172/1749902